

Orbital-Specific Modeling of CO Chemisorption

Sara E. Mason, Ilya Grinberg and Andrew M. Rappe

The Makineni Theoretical Laboratories, Department of Chemistry

University of Pennsylvania, Philadelphia, PA 19104-6323

(Dated: February 8, 2020)

Abstract

We demonstrate that variations in molecular chemisorption energy on different metals, different surface terminations, and different strain conditions can be accounted for by orbital-specific changes in the substrate electronic structure. Our density functional theory data set, spanning three metals, two surface terminations, and five strain states, is fit to a single model based on tight binding. A crucial aspect of the model is decomposition of the d -band into contributions from the five d atomic orbitals. This provides a representation of the energy levels of the substrate that are directly relevant to the chemisorption bond, leading to accurate prediction of chemisorption trends.

Currently, great attention is focused on elucidating how surface modification affects surface reactivity. [1, 2, 3, 4, 5] Recent research shows that small changes in surface electronic structure, induced by alloying or strain, can significantly change surface-catalyzed reaction rates. [6] A quantitative understanding of how changes in surface geometry and electronic structure affect surface reactivity will enable the design of more specific and more effective catalysts. It has been shown that ϵ_d , the center of the transition metal (TM) d -band density of states projected on the surface atoms (PDOS), is generally predictive of trends in chemisorption energies (E_{chem}) on TM surfaces. [7, 8, 9] However, quantitative accuracy (model predictions accurate within 0.1 eV) is still elusive, and for several cases there is poor or no correlation between ϵ_d and E_{chem} . [10, 11, 12] In this paper, using CO chemisorption as an example, we show that more rigorous examination of the surface electronic structure coupled with a simple modification of current chemisorption modeling enables us to achieve this goal.

We have compiled a database of DFT molecular top site (E_{chem}) and dissociative bridge site (E_{dissoc}) chemisorption energies and electronic structure measurements for CO on Pt, Pd, and Rh (111) and (100) surfaces. E_{chem} and E_{dissoc} are determined for each surface at the preferred theoretical lattice constants as well as under in-plane strains of $\pm 1\%$ and $\pm 2\%$, a range easily achievable through epitaxial mismatch. [13] Studying the response of chemisorption to strain as well as to different metals and facets deepens the study. Strain induces relatively subtle changes in E_{chem} and E_{dissoc} (compared to changes in metal or facet), so accurately accounting for large and small changes is a stringent test of a proposed theoretical model. Since lateral stress changes inter-planar separations, straining the systems also probes the interplay between in-plane and inter-plane perturbations to the surface geometry.

For each metal, surface, and strain state, two values for E_{chem} are determined, $E_{\text{chem}}^{\text{fix}}$ and $E_{\text{chem}}^{\text{rlx}}$. The former is the energy gain when the same chemisorption geometry is fixed over the relaxed bare surface for all metals and surfaces. In the latter, full ionic relaxation is allowed in the top two metal surface layers and all C and O ionic degrees of freedom. For the dissociative systems, we only determine $E_{\text{dissoc}}^{\text{fix}}$, due to the known instability of C and O atomic adsorption at bridge sites [14].

We focus attention on top-site E_{chem} and bridge-site E_{dissoc} for clarity. The symmetries at these sites provide for zero overlap between some d orbitals and the adsorbate orbitals,

making a clear distinction between orbital-specific and orbital-averaged models. Analysis of the top site also facilitates separation of the molecular chemisorption into σ and π contributions. However, even at low-symmetry sites, the contributions of the five d orbitals to chemisorption are unequal, making our orbital-specific treatment more accurate in general.

DFT calculations are performed with a generalized-gradient approximation (GGA) exchange-correlation functional [15] and norm-conserving optimized pseudopotentials [16] with the designed nonlocal method for metals. [17, 18] Pseudopotentials were designed using the OPIUM pseudopotential package. [19] All E_{chem} values have been corrected using our first-principles extrapolation procedure. [20] Metal surfaces are modeled as slabs of five layers separated by vacuum, with the $c(4 \times 2)$ surface cell for (111) surfaces and the $p(2 \times 2)$ surface cell for (100). CO top site and C and O bridge site chemisorption are modeled at coverage of $\Theta=1/4$. Calculations are done, and values of E_{chem} tested to be converged within 0.02 eV, using an $8 \times 8 \times 1$ grid of Monkhorst-Pack k -points, reduced by symmetry where possible. [21]

The PDOS for each orbital is constructed by projecting each atomic valence pseudowavefunction (radial wavefunction multiplied by real combination of spherical harmonics) of the surface atoms onto all the Kohn-Sham orbitals. Values of ϵ_d are then calculated as the first moment of each PDOS.

To reduce PDOS contributions from neighboring surface atoms, projection is performed within a sphere of radius r_{cut} centered about the surface atom of interest. Standard practice is to use a constant value for r_{cut} when comparing the PDOS and associated ϵ_d values of different surfaces, and $r_{\text{cut}} = 2$ a.u. is the default in some widely used DFT packages. [22, 23, 24] However, this approach leaves significant contributions from the orbitals of other atoms, making the calculated value of ϵ_d dependent on r_{cut} , which is undesirable.

To eliminate contamination from the orbitals of neighboring atoms, we evaluated ϵ_d at various r_{cut} values. (When $r_{\text{cut}} < 0.5$ a.u., the number of FFT grid points is too small to allow spherical sampling, so data are presented for $r_{\text{cut}} \geq 0.6$ a.u.) Figure 1 shows the variation of ϵ_d with r_{cut} for Pt(111) and Pt(100). It is apparent that the asymptotic behavior of ϵ_d is not reached until $r_{\text{cut}} \ll 2$ a.u. Furthermore, ϵ_d values for different surfaces, strain states and orbital angular momenta depend differently on r_{cut} . To obtain accurate ϵ_d values, we fit a purely quadratic function to the data and extrapolate ϵ_d to $r_{\text{cut}} = 0$. This procedure greatly reduces the contribution from the orbitals of neighboring atoms, making comparison

of ϵ_d for various systems more meaningful.

While our data confirm that E_{chem} qualitatively tracks with ϵ_d for the (111) surfaces, they reveal shortcomings of using ϵ_d for modeling bonding on different facets. From Figure 2, we see that E_{chem} values on different facets differ by 0.06–0.25 eV (0.15–0.85 eV for E_{dissoc}) even though they have the same ϵ_d and the same metal. Figure 2 and Table I show this is still true for ϵ_d with $r_{\text{cut}} \rightarrow 0$ a.u. Therefore, neither $E_{\text{chem}}^{\text{fix}}$ nor $E_{\text{dissoc}}^{\text{fix}}$ can be fit as a single function of ϵ_d , when both (111) and (100) facets are considered.

By contrast, we find that facet dependence of the chemisorption energies can be fit as a single linear function of ϵ_{xxyz} , the band center of the d_{xz} and d_{yz} orbitals. Figure 2 shows that single linear regressions of data for both facets are accurate to within 0.05 eV in all cases. This result demonstrates that focusing on the metal orbitals involved in bonding simplifies the observed chemisorption behavior and enables robust modeling.

Similarly, Table I shows that the response of E_{chem} and E_{dissoc} to strain is reflected in ϵ_{xxyz} but not ϵ_d . The tunability of E_{chem} and E_{dissoc} through strain is two to ten times greater on the (111) surfaces. However, $d\epsilon_d/ds$ is identical within computational precision for the two facets of each metal, so $d\epsilon_d/ds$ is uncorrelated with dE_{chem}/ds and dE_{dissoc}/ds . The chemisorption tunability trend is strongly reflected in $d\epsilon_{xxyz}/ds$, suggesting that the response of the d_{xz} and d_{yz} orbitals plays a key role in modeling top-site molecular and bridge-site dissociative adsorption of CO.

TABLE I: $E_{\text{chem}}^{\text{fix}}$, $E_{\text{chem}}^{\text{rlx}}$, $E_{\text{dissoc}}^{\text{fix}}$, ϵ_d , and ϵ_{xxyz} in eV for the (111) and (100) surfaces of Pt, Rh, and Pd. The slope of each quantity with respect to in-plane strain, ($\frac{d}{ds}$), is also reported, in units of meV/%strain. (ϵ_d and ϵ_{xxyz} use $r_{\text{cut}} \rightarrow 0$ a.u.)

	$E_{\text{chem}}^{\text{fix}}$	$\frac{dE}{ds}$	$E_{\text{chem}}^{\text{rlx}}$	$\frac{dE}{ds}$	$E_{\text{dissoc}}^{\text{fix}}$	$\frac{dE}{ds}$	ϵ_d	$\frac{d\epsilon}{ds}$	ϵ_{xxyz}	$\frac{d\epsilon}{ds}$
Pt(111)	-1.49	-36	-1.58	-46	1.99	-158	-1.77	20	-1.74	18
Pt(100)	-1.69	-3	-1.81	-5	1.03	-65	-1.76	20	-1.63	7
Rh(111)	-1.56	-27	-1.68	-24	0.48	-120	-1.38	31	-1.35	25
Rh(100)	-1.65	-18	-1.74	-9	0.11	-74	-1.36	29	-1.28	14
Pd(111)	-1.23	-25	-1.26	-29	1.66	-70	-1.58	32	-1.54	26
Pd(100)	-1.32	-5	-1.36	-6	1.50	-29	-1.56	19	-1.50	9

To explain the observed trends in E_{chem} as the metal identity, facet, and strain state

are varied, we reconsider the model for CO chemisorption. A second-order perturbative picture of chemisorption involving interacting molecular and metal orbitals is simple and intuitive, and has been known for some time. [25, 26] Hammer, Morikawa, and Nørskov (HMN) achieved significant success modeling molecular interactions with solid surfaces with a single perturbative term involving ϵ_d , the d -band center. [7] Guided by the trends presented above, we cast an orbital-specific analysis (OS) in the HMN model form, modeling top-site chemisorption as a perturbative interaction between molecular orbitals and the d -band PDOS of each spatial orbital:

$$E_{\text{chem}}^{\text{OS}} = E_{sp} - 4 \left\{ \frac{fV_{\pi}^2}{\epsilon_{2\pi^*} - \epsilon_{xxyz}} + fS_{\pi}V_{\pi} \right\} - 2 \left\{ \frac{(1-f)V_{\sigma}^2}{\epsilon_{z^2} - \epsilon_{5\sigma}} + (1+f)S_{\sigma}V_{\sigma} \right\} \quad (1)$$

where f is the idealized filling of the metal d bands, V and S are perturbation matrix elements and overlap integrals, respectively, labeled by symmetry, $\epsilon_{2\pi^*}$ and $\epsilon_{5\sigma}$ are the CO molecular orbital energies, ϵ_{xxyz} , the band center of the d_{xz} and d_{yz} orbitals and ϵ_{z^2} is the band center of the d_{z^2} orbitals. [30] As in the original HMN model, α and β are introduced as fitting parameters common to all metals, and $V_{\pi}^2 \approx \beta V_{sd}^2$ and $S_{\pi} \approx -\alpha V_{\pi}$. From our analysis of DFT orbitals, we find that S_{σ}/S_{π} to be sensitive in the limit of desired accuracy to both metal identity and adsorption geometry. Our overlap analysis gives S_{σ}/S_{π} is 1.182, 1.156, and 1.200 for Pt, Rh, and Pd, respectively. E_{sp} is found to be -0.15 eV from DFT calculations on Al surfaces [27] and assumed to be independent of metal identity, facet, or strain. For the (111) and (100) surfaces, we find that f for each of the decomposed d -bands is well approximated by the idealized filling of the metal d -bands, $f = (\nu - 1)/10$, where ν is the valence of the metal atom.

The corresponding conventional orbital-averaged (OA) model form is given by:

$$E_{\text{chem}}^{\text{OA}} = E_{sp} - 4 \left\{ \frac{fV_{\pi}^2}{\epsilon_{2\pi^*} - \epsilon_d} + fS_{\pi}V_{\pi} \right\} - 2 \left\{ \frac{(1-f)V_{\sigma}^2}{\epsilon_d - \epsilon_{5\sigma}} + (1+f)S_{\sigma}V_{\sigma} \right\} \quad (2)$$

We fit the data for both fix and rlx chemisorption systems to the Equation 1 and Equation 2. [31] Figure 3 shows the correlation between DFT and model values for the more realistic rlx chemisorption systems. We calculate the root-mean-square error (RMSE) as

an evaluation of the model, considering the (111) and (100) data separately and combined. When Equation 2 is used to fit the data, the RMSE is 0.051 and 0.100 eV for the (111) and (100) surfaces respectively, and 0.079 eV overall. When Equation 1 is used to fit the data, the RMSE is 0.052 and 0.051 eV for the (111) and (100) surfaces respectively, and 0.052 eV overall. This shows that the more sophisticated model form of Equation 1 is required to achieve the same level of accuracy for these two surfaces.

We now address why different levels of model sophistication are needed to achieve the same accuracy in predicted E_{chem} on the (111) and (100) surfaces. First, we consider the salient electronic structure differences between the (111) and (100) surface facets. The dd metal bonding can be decomposed by symmetry into σ , π , and δ contributions. [28] The square lattice of the (100) surface allows for strong $dd\sigma$ overlap between neighboring $d_{x^2-y^2}$ orbitals. Our DFT data show that $\epsilon_{x^2-y^2}$ is significantly lower on (100) surfaces than on (111), as shown for Pt in Figure 1. Since (100) surface atoms have eight nearest neighbors while the (111) atoms have nine, the other d orbitals are less stable on (100) surfaces to varying extents, with ϵ_{xz} and ϵ_{yz} significantly higher on (100) than (111). Averaging all the d orbitals causes the rise in bonding-relevant ϵ_{xz} and ϵ_{yz} to be masked by the drop in bonding-irrelevant $\epsilon_{x^2-y^2}$, so that even though ϵ_{xxyz} closely tracks the increase in E_{chem} on the (100) surface relative to the (111) surface, the averaged ϵ_d does not.

When tensile strain is applied to a TM surface, the weakened in-plane bonding destabilizes the d orbitals. ϵ_d shifts upward, leading to stronger E_{chem} . [7] This basic prediction was confirmed in the DFT study of Mavrikakis *et al.* [9] However, different d orbitals shift by different amounts, based on their orientations relative to the surface.

In addition, the inter-planar spacing between the top two metal layers (r_{12}) responds to the strain, and this further affects substrate electronic structure, again in an orbital-specific way. Tensile lateral strain usually decreases r_{12} , while compression increases r_{12} . The bonding-relevant d_{xz} and d_{yz} orbitals of the top layer have the strongest interaction with the second layer atoms, so the relaxation of r_{12} significantly reduces the effect of lateral strain for these orbitals. This is why $d\epsilon_{xxyz}/ds$ is less than $d\epsilon_d/ds$ for all surfaces studied (Table I).

The effect of r_{12} relaxation on strain tunability is also strongly facet-dependent. On the more open (100) surface, relaxations of r_{12} are larger, making $d\epsilon_{xxyz}$ smaller for each (100) facet studied than for the corresponding (111) facet. This explains why the tunability of

E_{chem} (fix and rlx) and $E_{\text{dissoc}}^{\text{fix}}$ are much lower on (100) surfaces than on (111) surfaces.

Our demonstration that a single orbital-specific chemisorption model can be applied to different facets, strains, and metals, has implications for the modeling and design of more realistic catalyst surfaces. DFT studies have found that reactions on late TMs are more likely to proceed on defects such as steps and kinks. [29] The model presented suggests that one should examine how different nearest-neighbor and inter-planar separations affect the orbital-specific electronic structure, and predict chemisorption properties accordingly.

Incorporating the effects of strain and r_{12} relaxation on the relevant PDOS centers greatly improved chemisorption modeling. We therefore suggest that if further couplings between PDOS centers and adsorbate structure can be parameterized, the resulting model could offer even greater accuracy and broader applicability.

In conclusion, we use the energy levels of the substrate d -band projected onto the substrate atomic orbitals and their overlap with the CO bonding molecular orbitals, in a second-order perturbation theory-type model for chemisorption. The resulting model is able to account for changes in E_{chem} on different surface facets under different conditions of strain. We have also shown that trends in the dissociative chemisorption of CO at bridge site are governed by the same orbital-specific factors. The results shown here should be generally valid for other molecular and atomic adsorption on higher index surfaces and for perturbations other than strain.

This work was supported by the Air Force Office of Scientific Research, Air Force Materiel Command, USAF, under grant number FA9550-04-1-0077, and the NSF MRSEC Program, under Grant DMR05-20020. Computational support was provided by the Defense University Research Instrumentation Program, and the High Performance Computing Modernization Office of the Department of Defense. SEM acknowledges Valentino R. Cooper for fruitful exchange of ideas.

- [1] M. Gsell, P. Jakob, and D. Menzel, *Science* **280**, 717 (1998).
- [2] M. K. Rose, T. Mitsui, J. Dunphy, A. Borg, D. F. Ogletree, M. Salmeron, and P. Sautet, *Surf. Sci.* **512**, 48 (2002).
- [3] A. Schlapka, M. Lischka, A. Groß, U. Käsberger, and P. Jakob, *Phys. Rev. Lett.* **91**, 016101

(2003).

- [4] J. R. Kitchin, J. K. Nørskov, M. A. Bartheau, and J. G. Chen, Phys. Rev. Lett. **93**, 156801 (2004).
- [5] F. Abild-Pedersen, J. Greeley, and J. K. Nørskov, Catal. Lett. **105**, 9 (2005).
- [6] T. Bligaard, J. K. Nørskov, S. Dahl, J. Matthiesen, C. H. Christensen, and J. Sehested, J. Catal. **224**, 206 (2004).
- [7] B. Hammer, Y. Morikawa, and J. K. Nørskov, Phys. Rev. Lett. **76**, 2141 (1996).
- [8] B. Hammer, O. H. Nielsen, and J. K. Nørskov, Catal. Lett. **46**, 31 (1997).
- [9] M. Mavrikakis, B. Hammer, and J. K. Nørskov, Phys. Rev. Lett. **81**, 2819 (1998).
- [10] C. Lu, I. C. Lee, R. I. Masel, A. Wieckowski, and C. Rice, J. Phys. Chem. A **106**, 3084 (2002).
- [11] Z. P. Liu, J. J. Stephen, and D. A. King, J. Amer. Chem. Soc. **126**, 10746 (2004).
- [12] V. R. Cooper, A. M. Kolpak, Y. Yourdshahyan, and A. M. Rappe, Phys. Rev. B Rapid Comm. **72**, 081409(R) (2005).
- [13] J. Hrbek and R. Q. Hwang, Curr. Opin. Solid State Matter. Sci. **5**, 67 (2001).
- [14] D. C. Ford, Y. Xu, and M. Mavrikakis, Surf. Sci. **587**, 159 (2005).
- [15] J. P. Perdew, K. Burke, and M. Ernzerhof, Phys. Rev. Lett. **77**, 3865 (1996).
- [16] A. M. Rappe, K. M. Rabe, E. Kaxiras, and J. D. Joannopoulos, Phys. Rev. B Rapid Comm. **41**, 1227 (1990).
- [17] N. J. Ramer and A. M. Rappe, Phys. Rev. B **59**, 12471 (1999).
- [18] I. Grinberg, N. J. Ramer, and A. M. Rappe, Phys. Rev. B Rapid Comm. **63**, 201102(R) (2001).
- [19] <http://opium.sourceforge.net>.
- [20] S. E. Mason, I. Grinberg, and A. M. Rappe, Phys. Rev. B Rapid Comm. **69**, 161401(R) (2004).
- [21] H. J. Monkhorst and J. D. Pack, Phys. Rev. B **13**, 5188 (1976).
- [22] X. Gonze, J.-M. Beuken, R. Caracas, F. Detraux, M. Fuchs, G.-M. Rignanese, L. Sindic, M. Verstraete, G. Zerah, F. Jollet, et al., Comp. Mater. Sci. **25**, 478 (2002).
- [23] <http://www.abinit.org/>.
- [24] <http://dcwww.camp.dtu.dk/campos/Dacapo/>.
- [25] R. Hoffman, Rev. Mod. Phys. **60**, 601 (1988).
- [26] G. Blyholder, J. Phys. Chem. **68**, 2772 (1964).
- [27] S. E. Mason, I. Grinberg, and A. M. Rappe, J. Phys. Chem. B (2006),

<http://dx.doi.org/10.1021/jp0548669>.

- [28] A. P. Sutton, *Electronic Structure of Materials* (Oxford University Press, 1993).
- [29] Z.-P. Liu and P. Hu, *J. Am. Chem. Soc.* **125**, 1958 (2003).
- [30] Taking the top site as an example, $S_{\pi,i} \neq 0$ for d_{xz} and d_{yz} only, and $S_{\sigma,i} \neq 0$ for d_{z^2} . HMN values of $\epsilon_{2\pi^*}=2.5$ eV and $\epsilon_{5\sigma}=7$ eV are used. Moderate changes to these values re-scales the dependence of E_{chem} on ϵ_d without significantly changing any presented results.
- [31] For the fix data, the best fit to Equation 1 is achieved when $\alpha=0.0619$ eV and $\beta=1.052$ eV², and the best fit to Equation 2 is achieved when $\alpha=0.0578$ eV and $\beta=0.938$ eV². For the rlx data, the best fit to Equation 1 is achieved when $\alpha=0.0619$ eV and $\beta=1.050$ eV², and the best fit to Equation 2 is achieved when $\alpha=0.0604$ eV and $\beta=1.048$ eV².

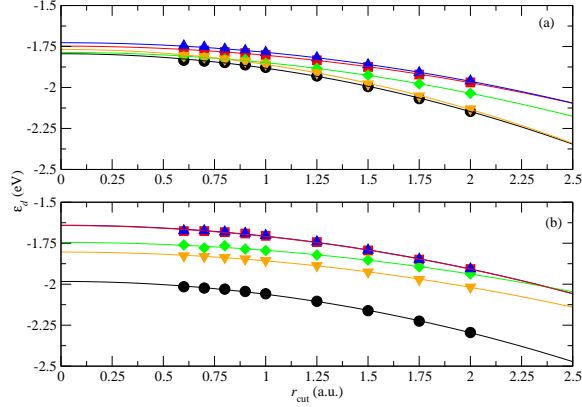


FIG. 1: (a) Variation in ϵ_d as a function of projection sphere cutoff radius r_{cut} for Pt(111). $\epsilon_{x^2-y^2}$, ϵ_{xz} , ϵ_{z^2} , ϵ_{yz} , and ϵ_{xy} PDOS centers are shown by circles, squares, diamonds, up-triangles, and down-triangles, respectively. (b) Same as (a) for Pt(100).

The graphs demonstrate the importance of extrapolating $r_{\text{cut}} \rightarrow 0$ a.u.: for Pt(111) the asymptotic d -band centers are more nearly equal than their large- r_{cut} estimates; for Pt(100) they are more dissimilar.

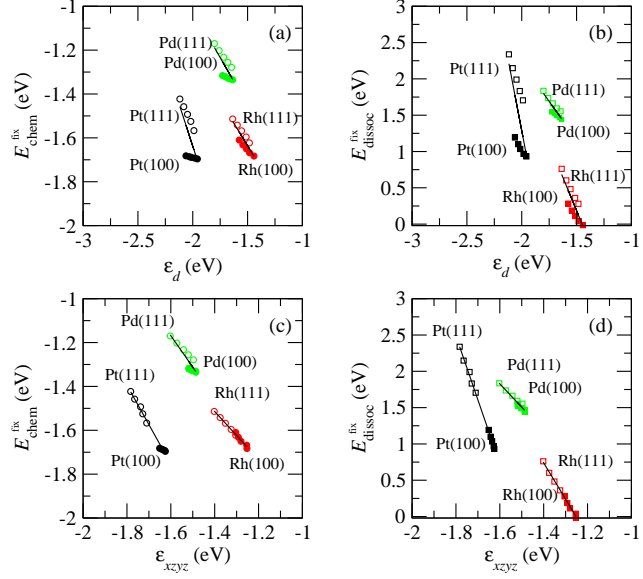


FIG. 2: Plots of $E_{\text{chem}}^{\text{fix}}$ and $E_{\text{dissoc}}^{\text{fix}}$ vs. ϵ_d and ϵ_{xzyz} for Pt (circle), Rh (square), and Pd (diamond) (111) surfaces (open) and (100) surfaces (filled). Data for five lateral strain states (0%, $\pm 1\%$, and $\pm 2\%$) are shown. Linear regressions are shown for each metal. (a) $E_{\text{chem}}^{\text{fix}}$ vs. ϵ_d , $r_{\text{cut}}=2$ a.u. (b) $E_{\text{dissoc}}^{\text{fix}}$ vs. ϵ_d , $r_{\text{cut}}=2$ a.u. (c) $E_{\text{chem}}^{\text{fix}}$ vs. ϵ_{xzyz} , $r_{\text{cut}} \rightarrow 0$ a.u. (d) $E_{\text{dissoc}}^{\text{fix}}$ vs. ϵ_d and ϵ_{xzyz} , $r_{\text{cut}} \rightarrow 0$ a.u.

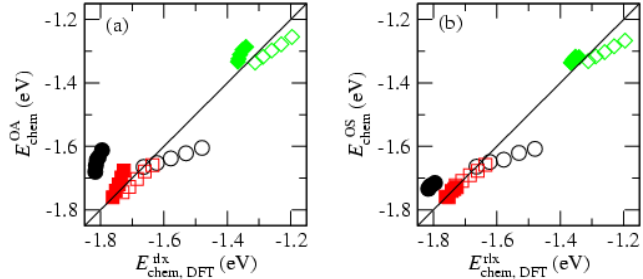


FIG. 3: Correlation plots of modeled E_{chem} and $E_{\text{chem,DFT}}$. Pt (circle), Rh (square), and Pd (diamond) (111) surfaces (open) and (100) surfaces (filled). Data for five lateral strain states (0%, $\pm 1\%$, and $\pm 2\%$) are shown. (a) $E_{\text{chem}}^{\text{OA}}$ (Equation 2) vs. $E_{\text{chem,DFT}}^{\text{rlx}}$. (b) $E_{\text{chem}}^{\text{OS}}$ (Equation 1) vs. $E_{\text{chem,DFT}}^{\text{rlx}}$.

The plots show that orbital-specific modeling (Equation 1) is required to achieve the same quality of correlation for both (111) and (100) facets.